Biogeochemistry of Carbon in the Amazonian Floodplains over a 2000-km Reach: Insights from a Process-Based Model

Vincent Bustillo,*,+ Reynaldo Luiz Victoria,# Jose Mauro Sousa de Moura,@ Daniel de Castro Victoria,& Andre Marcondes Andrade Toledo, and Erich Colicchio++**

+Centro de Energia Nuclear na Agricultura, Laboratório de Geoprocessamento e Tratamento de Imagens, Piracicaba, Brazil, and Université François Rabelais de Tours, UMR CNRS/INSU 6113 Institut des Sciences de la Terre d'Orléans, Université d'Orléans, Tours, France
#Centro de Energia Nuclear na Agricultura, Laboratório de Geoprocessamento e Tratamento de Imagens, and USP–ESALQ, NUPEGEL, Piracicaba, Brazil
@Universidade Federal do Oeste do Para, Santarem, Brazil
&Embrapa Monitoramento por Satélite, Campinas, Brazil
**Universidade Federal de Mato Grosso, Rondonópolis, Brazil
++Universidade Federal do Tocantins, AgroUnitins, Palmas, Brazil

Received 13 March 2010; accepted 16 September 2010

ABSTRACT: The influence of Amazonian floodplains on the hydrological, sedimentary, and biogeochemical river budget was investigated over a 2000-km reach. A process-based model relying on the closure of chemical fluxes and isotopic signals was implemented. On average for the whole studied reach, the overall fluxes of carbon associated with mineralization and aquatic photosynthesis were estimated to 35.7 and 15.3 Tg C yr^{-1}, respectively. Almost 57% of the carbon sequestrated by photosynthesis comes from aerial sources (flooded

* Corresponding author address: Vincent Bustillo, Université François Rabelais de Tours, Parc Grandmont, UFR Sciences et Techniques, Bâtiment E, 37200 Tours, France.
E-mail address: bustillovincent@hotmail.com

DOI: 10.1175/2010EI338.1

forest); the remaining 43% resulted from aquatic sources (várzea grasses and phytoplankton). The process rates substantially fluctuate over the annual cycle, depending particularly on the extension of flooded area and on the river–floodplain connectivity. As the river level declines, the drastic decrease of turbidity and the lower supply of carbon substrates promote autotrophy to the detriment of heterotrophy, leading to substantial changes of pH and gaseous equilibria in the river water. The main consequences are (i) the side-chain oxidation of dissolved organic matter leading to the concomitant rises of the carbon to nitrogen atomic ratio and nitrate contents and (ii) the sorption of hydrophobic humic acids, which fractionate ^{13}C and thus lead to ^{13}C-depleted particulate organic matter (fine fraction) compared to remaining dissolved organic matter. As the river flow rises, the heterotrophy prevails over autotrophy and this tends to attenuate the chemical signature imprinted by the latter. The significant contribution of aerial autochthonous sources to the budget of carbon indicates that the fluxes of mineralization are sustained by the net primary production of river corridors. The variable extension of submerged areas defines the proportions of CO_2 exported by the river and released to the atmosphere. The rate of CO_2 outgassing on the studied reach (18.8 Tg C yr^{-1}) represents about 50% of the incoming dissolved inorganic carbon flux. The rate of methane emission is estimated as 2.2 Tg C yr^{-1} and that of denitrification is estimated as 0.87 Tg N yr^{-1}, representing 1.5 times the flux of dissolved inorganic nitrogen (DIN) exported by the Amazon River at the station of Óbidos (0.64 Tg N yr^{-1}).

KEYWORDS: Amazon River; Floodplains; Biogeochemical cycles; Carbon; CO_2 outgassing

1. Introduction

This paper focuses on the quantification of processes driving the biogeochemical budget of carbon within the Amazonian floodplains (FP) over a 2000-km reach extending between the stations of Vargem Grande (VG; upstream boundary) and Óbidos (Óbi; downstream boundary). The Amazonian forest is commonly considered to be a very significant sink of carbon because of the storage capacity of soils (Bernoux et al. 2002) and biomass (Brown and Lugo 1992). Scientific investigations on the Amazon River demonstrate that flooded areas constitute very important sources of carbonaceous greenhouse gases, involving not only CO_2 (Richey et al. 1988; Richey et al. 2002) but also CH_4 (Devol et al. 1988). The strong seasonality of the Amazon River discharge promotes changes in stage height of as much as 10 m (Richey et al. 1989; Mayorga and Aufdenkampe 2002), thus determining very significant changes in the extent of flooded areas within the central lowlands: from 100 000 km^2 in November to 350 000 km^2 in May (Richey et al. 2002). According to these authors, the rivers of Central Amazonia (quadrant of 1.77×10^6 km^2) return about 210 Tg C yr^{-1} as carbon dioxide to the atmosphere. Mayorga et al. (Mayorga et al. 2005) showed that this outgassing flux of carbon dioxide was driven by the respiration of terrestrial organic carbon that is less than 5 years old and mainly composed of autochthonous sources (várzea grasses), as stated previously by Quay et al. (Quay et al. 1992).

Recently, the River Basin Organic Matter and Biogeochemistry Synthesis (ROMBUS) model was implemented by Richey et al. (Richey et al. 2004) to decipher the complex signals from dissolved organic matter (DOM) of variable molecular size. Within ROMBUS, each of the organic and inorganic carbon pools

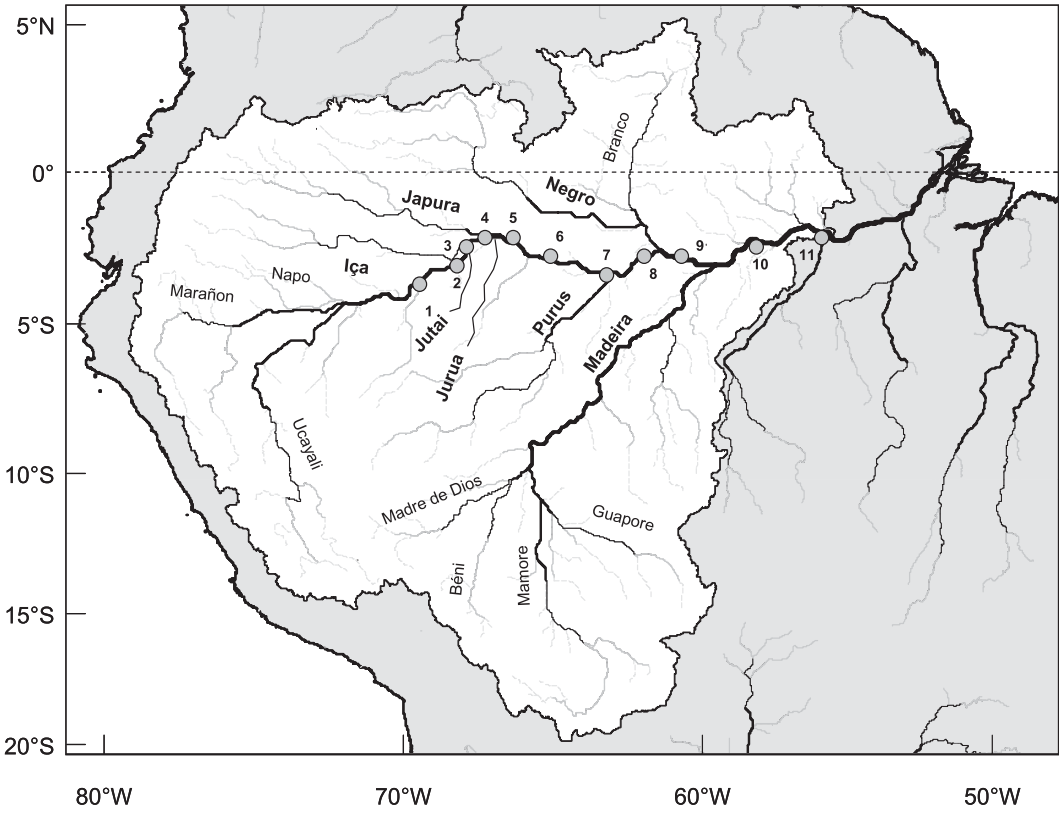

Figure 1. Map of the Amazon River basin and location of the main tributaries. The sampling stations are 1) VG, 2) Santo Antonio do Içá, 3) Xibeco (Xib), 4) Tupe (Tup), 5) Jut, 6) Ita, 7) Anori (Ano), 8) Man, 9) São Jose da Amatari (SJA), 10) Pau, and 11) Óbi.

is represented by state variables that characterize the nitrogen-to-carbon ratio (for the OM pools), $\delta^{13}C$ signature, and age (via $\Delta^{14}C$). A survey of the spatial and temporal variability in $\Delta^{14}C$ signatures of different carbon fractions was performed 1) to investigate the biogeodynamics of carbon in Amazonian river of differing types and sizes and 2) to constrain better age, turnover, and pathways of these principal carbon fractions for the implementation and validation of a new ROMBUS model. In this context, the implementation of a process-based model, including all carbon fractions, is potentially of great interest to quantify the magnitude of processes driving the biogeodynamics of carbon within the river system and at its interfaces with the atmosphere and with the sediment.

1.1. Preliminary work

Biogeochemical mass balances were established (Bustillo et al. 2010) by comparing incoming and outgoing mass balances at 10 monitoring stations (Figure 1) located along the studied fluvial reach. Six end-member mixing models were implemented to revisit the interpretations given to the seasonally structured excesses

and deficits with respect to inputs and outputs. By comparing the outputs of many different models designed for different purposes, the nature and the magnitude of processes linking water and biogeochemical budgets of the Amazonian floodplains were clarified. Each one provides a specific insight on the soil–river system dynamics by coupling hydrological, sedimentary, and biogeochemical budgets. The comparison of the model outputs, and the analysis of their reciprocal consistency, enabled us to decipher much more assuredly the nature and magnitude of processes occurring in the floodplains. These are mixing models based on 1) variable regional sources with and without correction of inputs by small tributaries; 2) variable hydrological sources with three end members to determine their individual compositional evolution, with contrasted response depending on hydrograph stage, throughout their course in the floodplains; 3) variable hydrological sources with three end members, including a correction on the baseflow to account for in-stream biogenic transformations; and 4) mixed approaches combining the regional variability of five chemical signals (between river basins) and the variability related to the hydrological source (between contributing runoffs or endmembers), taking into consideration the defaults of floodplains water balance. These models enabled us to identify the main factors (hydrological source, water budget of the floodplains, nature of hydrobiological pattern; i.e., photosynthesis versus mineralization, air–water gaseous exchanges, etc.) controlling the biogeochemical and sedimentary budgets of Amazonian floodplains.

This study revealed that most of the chemical baseline of the Amazon River basin was acquired before the studied 2000-km Amazonian reach. However, the tight connection between the hydrograph stage of the river and the chemical signals provided insightful information on the dynamics of its floodplains. The chemical expression of biotic and abiotic processes occurring in the Amazonian floodplains can be more easily identified during falling waters. It appears delayed in time compared to the maximum extension of submerged area because the alternating water circulation direction (filling versus emptying) between the main channel (MC) and the adjacent floodplains determines delayed emptying of floodplains during falling waters. It results also in a longer residence time in the hydrograph network, which strengthens the rate of transformation of transiting materials and solutes. Biotic and biologically mediated processes tend to accentuate changes in river water chemistry initiated upstream, in each subbasin, along river corridors, indicating that processes operating downstream prolong those from upstream (e.g., floodplains of the large tributaries). Conversely, the flood wave propagation tends to lessen the seasonal variability as a result of the water storage in the floodplains, which admixes waters of distinct origins (in time and space). The morphology of floodplains, determining the deposition and the diagenesis of the sediments as well as the variable extension of submerged areas or the chronology of floodplains storage/emptying, appears to be the main factor controlling the biogeodynamics of the floodplains. By coupling classical end-member mixing models (providing insight on hydrological source) with a variable regional contribution scheme, relevant information on the biogeochemical budget of the Amazonian floodplains could be captured. However, the identification, magnitude, and chronological succession of major processes driving the biogeochemistry of carbon were not completely elucidated. Therefore, this paper aims to bridge the knowledge gap by testing a process-based model constrained by chemical and isotopic data.

1.2. Organization of the paper

In light of the results of the six mixing models, two main issues dealing with the biogeochemistry and hydrology of floodplains are addressed:

1) nature, magnitude, and seasonal fluctuations of biotic processes (autotrophy versus heterotrophy) and
2) nature and magnitude of abiotic processes involving notably the sorption of dissolved organic matter and the gaseous exchanges at the air–water interface.

This paper aims to investigate more in detail these two topics, which are intrinsically related and determine most of the biogeochemical budget of the Amazonian floodplains with respect to carbon and nitrogen. To achieve this objective, a process-based model describing the balance of the chemical and isotopic budgets of C, N, and O was implemented. This model relies on the classical survey of river water chemistry through the Carbon in the Amazon River Experiment (CAMREX). Specifically, the process-based model requires the assimilation of appropriate in-field studies or remote sensing data to constrain chemical and isotopic budgets. The new modeling approach, implemented here, provides an original and pertinent framework to appreciate quantitatively and qualitatively the biogeochemical budget of carbon over a 2000-km reach. Over the last three decades, a considerable amount of field data were collected, but few studies using the whole dataset of the CAMREX project are based on a modeling approach. We propose here to gather the very valuable amount of information provided by the CAMREX project and its extensions [e.g., Large-scale Biosphere-Atmosphere Experiment in Amazonia (LBA)] to implement a comprehensive process-based model of carbon biogeochemistry at a very large scale.

The main originality of this study resides in the implementation of a modeling approach, constrained by a very large amount of chemical data. This model is expected to assimilate and synthesize this information, thus providing unique insight and quantified issues on the major processes that drive carbon and nitrogen biogeochemical budgets over a 2000-km reach.

2. Study area and available dataset

The Amazon River is the largest river in the world by discharge with a total river flow greater than the next eight largest rivers combined. Its drainage basin is the largest in the world, covering about 6 915 000 km^2 at its mouth. It gathers its waters from 5°N to 20°S. The quantity of water released by the Amazon to the Atlantic Ocean might exceed 300 000 $m^3\ s^{-1}$ during the rainy season (Mayorga and Aufdenkampe 2002). The Amazon is responsible for about 20% of the total volume of water entering the oceans worldwide. The confluence of Andean tributaries in the Amazonian plain gathers a considerable amount of water and generates huge discharges. The flatness of the Amazonian valley (2.1 cm km^{-1} between Vargem Grande and Óbidos) promotes the large-scale flooding of alluvial plains. During the wet season, some parts of the Amazon might reach 100 km in width. The area covered by the water of the Amazon River and its tributaries is multiplied by 3 over the course of a year: on average, during the dry season,

100 000 km^2 are flooded, whereas the water-covered area rises to 350 000 km^2 in the wet season. Because of its vast dimensions, the Amazonian FP constitutes an ideal open-sky laboratory for studying the dynamics of sediments, carbon species, biogenic species, and solutes, whose concentrations and mass balance change during their course throughout the floodplains. The study focuses on the 2000-km fluvial reach extending between Vargem Grande (upstream area = 10^6 km^2), close to the frontier between Peru and Brazil, and Óbidos (Amazon River, upstream area = 4.62×10^6 km^2), the outlet of the studied reach located 700 km landward from the mouth and where tidal influence remain low. Nine major tributaries join the Amazon main stem over this section: Içа, Japurá, and Negro on the northern side; Jutaí, Juruá, Purus, Negro, and Madeira on the southern side; and Solimões from the Peruvian Andes. A view of the Amazon River basin upstream from Óbidos, including the hydrograph network and the location of CAMREX's monitoring station along the Amazon River main stem, is presented in Figure 1.

The dataset used in this study is from the CAMREX project (1982–91). The objective of CAMREX project was to define by mass balances and direct measurements those processes that control the distribution of bioactive elements (C, N, P, and O) in the main stem of the Amazon River in Brazil. Representative flux-weighted water samples for comprehensive chemical analysis and for taking rate measurements were obtained over 18 different sites within a 2000-km reach of the Brazilian Amazon main stem, including major intervening tributaries. The CAMREX dataset represents a time series unique in its length and detail for very large river systems. Samples were collected on 13 different cruises (1982–91) during contrasting hydrographic stages, consisting in depth-integrated, discharge-weighted composite water samples (20–40 L). In this study, the samples from cruises 9–13 were not used because the chemical parameters required for modeling purposes were not all analyzed. The sampling and analytical procedures used during CAMREX were presented by Richey et al. (Richey et al. 1986), Hedges et al. (Hedges et al. 1986a), and Devol et al. (Devol et al. 1987). These will therefore be described only briefly. Materials in water were first separated into fractions by size. The three size classes (coarse, fine, and dissolved) display very distinct transport dynamics, degradation patterns, and compositional characteristics (Mayorga and Aufdenkampe 2002). Coarse particulate, fine particulate, and dissolved fractions were thus operationally defined using a sieve pore size of 63 μm to separate particulate fractions: coarse suspended sediments (CSS) versus fine suspended sediments (FSS) and filter pore sizes of 0.45 μm to isolate dissolved constituents. FSS was isolated by continuous-flow centrifugation. FSS consist of clays and silts, material between 0.45 and 63 μm in size as defined by CAMREX (Mayorga and Aufdenkampe 2002). Elemental compositions, reported as weight percentages of organic carbon and total nitrogen, were measured with a Carbo Erba model 1106 carbon, hydrogen, and nitrogen (CHN) analyzer within each size fraction. Related concentrations [particulate organic carbon (POC) and particulate organic nitrogen (PON) within fine (POCF and PONF) and coarse (POCC and PONC) size fractions] were then calculated as the product of weight measurement and suspended concentrations. Remaining material ($<$0.45 μm) constitutes the dissolved fraction (DOM), whose carbon content [dissolved organic carbon (DOC)] was measured using a potassium persulfate oxidation procedure. The concentration of dissolved inorganic carbon (DIC; μM) was established from

pH and alkalinity titration measurements. The $\delta^{13}C$ values for DIC, POCF, and POCC are reported versus marine carbonate [Pee Dee Belemnite (PDB) standard]. The measurements of ^{13}C:^{12}C were made with two mass spectrometers, a Nuclide 6–60 and Finnigan MAT 251.

One of the greatest strengths of the CAMREX database resides in the very wide spectrum of analyzed parameters: major ions (Na^+, K^+, Ca^{2+}, Mg^{2+}, HCO_3^-, SO_4^{2-}, and Cl^-; concentrations given in μM); organic species [DOC (mg L^{-1}; size $<$ 0.45 μm), DIC (μM), and particulate organic carbon (POC; mg L^{-1})]; suspended sediments (mg L^{-1}); dissolved organic nitrogen (DON; μM); NO_3^- (μM); NH_4^+ (μM); dissolved phosphorus (PO4; μM); total phosphorus (Pt; mg L^{-1}); particulate organic nitrogen (PON; mg L^{-1}); dissolved gases (O_2 and CO_2; μM); pH, alkalinity, and isotopic data for river water ($\delta^{18}O$; ‰ SMOW); and carbon species {$\delta^{13}C$ (‰; PDB) for dissolved inorganic carbon [DIC] = [HCO_3^-] + [CO_2] + [CO_3^{2-}], POCF, and POCC}. Note the absence of data for $\delta^{13}C$ (DOC) and NO_2^-, which would have been ideally required to better constrain carbon and nitrogen budgets. Available data correspond to cross-sectionally integrated samples. According to Quay et al. (Quay et al. 1992) and based on replicate analyses ($n = 3$) of the same sample, the precisions of the measurements ($\pm$1 standard deviation) were $\pm$1.5% for fine materials [fine particulate OM (FPOM) and FSS]; $\pm$3.0% for coarse materials [coarse particulate OM (CPOM) and CSS]; $\pm$3.0% for dissolved inorganic carbon; and $\pm$0.1‰ for $\delta^{13}C$ of FPOM, CPOM, and DIC.

The dataset, extracted from pre-LBA CD-ROM (Richey et al. 2008), constitutes, until that date, the basis of more than 130 CAMREX publications that have focused on understanding physical and biogeochemical dynamics throughout the basin using a large variety of approaches.

3. Modeling strategy

The modeling strategy consists in assessing the biogeochemical balance of carbon and nitrogen in the floodplains by constraining chemical and isotopic budget of carbon and nitrogen species. The imbalances between incoming (IN*) and outgoing (OUT) fluxes are interpreted as the result of several processes arising in the Amazon River. The composition of the incoming flux $C^{i,j}_{k,\mathrm{IN}*}$ is given by the discharge-weighted mixture of the waters coming from the n major tributaries located upstream from the jth sampling station (concentration $C^{i,j}_{k,M1}$ and total discharge upstream from the nth confluent $Q^j_{t,k} = \sum_{j=1}^{j=n} Q^j_{t,k}$) and those from ungauged areas (concentration $C^i_{k,\mathrm{UA}}$ and total discharge $Q^j_{k,\mathrm{UA}}$),

$$C^{i,j}_{k,\mathrm{IN}*} = \frac{C^{i,j}_{k,M1} \times Q^j_{t,k} + C^i_{k,\mathrm{UA}} \times Q^j_{k,\mathrm{UA}}}{Q^j_{t,k} + Q^j_{k,\mathrm{UA}}}. \quad (1)$$

The composition of the flow supplied by ungauged areas ($C^i_{k,\mathrm{UA}}$) is approximated by the composition of the Jutaí River (76 000 km^2), which was monitored along the eight cruises of the CAMREX project. This choice is consistent because lithological and hydroclimatological features of the Jutaí River basin are representative of those of ungauged areas (Tardy et al. 2009) and because the chemical composition and variability of the Jutaí River are in good agreement with those of black water rivers draining Central Amazonian area [e.g., see dataset from the

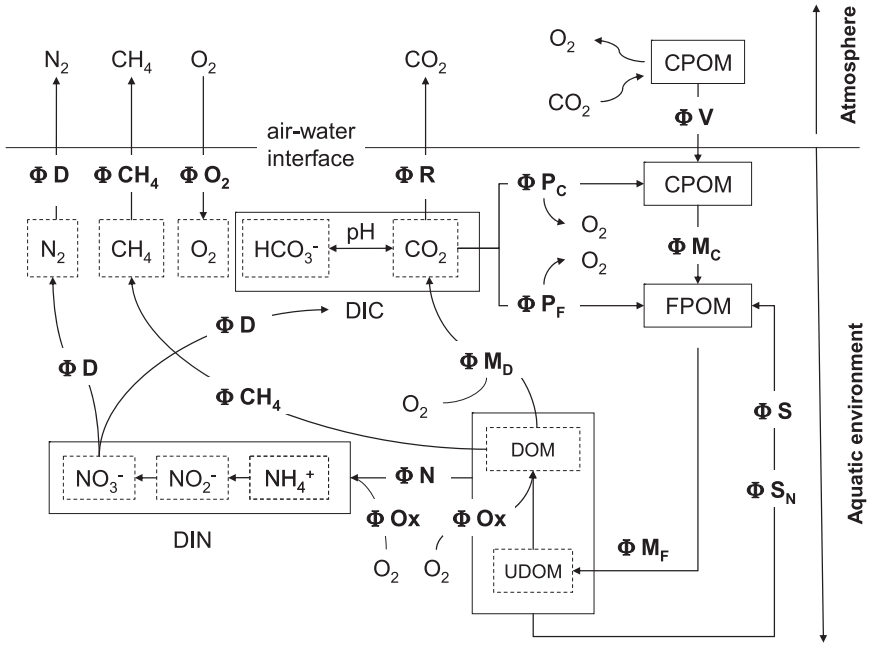

Figure 2. Overview of major processes driving C and N biogeodynamics in rivers.

Hydrology and Geochemistry of the Amazon Basin (HiBAm) project at the outlet of the Trombetas River]. The discharge of the ungauged area $Q^j_{k,\mathrm{UA}}$ is estimated by the difference between the outgoing discharge downstream from the nth major tributary ($Q^j_{k,\mathrm{OUT}}$) and the sum of discharge of the n major tributaries ($\sum_{j=1}^{j=n} Q^j_{t,k}$), leading to

$$Q^j_{k,\mathrm{UA}} = Q^j_{k,\mathrm{OUT}} - \sum_{j=1}^{j=n} Q^j_{t,k}. \tag{2}$$

The imbalances between IN* and OUT fluxes, noted $\Delta\Phi(C^j_{i,k})$, are calculated as follows:

$$\Delta\Phi(C^j_{i,k}) = [C^{i,j}_{k,\mathrm{OUT}} - C^{i,j}_{k,\mathrm{IN}*}] \times Q^j_{k,\mathrm{OUT}}, \tag{3}$$

where $C^{i,j}_{k,\mathrm{OUT}}$ is the concentration of the ith chemical specie observed at the jth sampling station for the kth cruise.

The process-based description of C and N biogeochemical cycles implies 14 river processes (Figure 2 and Table 1): nonaquatic (aerial) photosynthesis followed by the incorporation of newly formed organic matter in the aquatic environment (flux noted ΦV); aquatic photosynthesis removing DIC and dissolved inorganic nitrogen (DIN) to form POCC and PONC (flux noted ΦP_C); aquatic photosynthesis removing DIC and DIN to form POCF and PONF (flux noted ΦP_F); physical size reduction of coarse particulate organic matter CPOM through mechanical means (flux noted ΦM_c) releasing POCF and PONF without consuming O_2; physical size reduction of fine particulate organic matter FPOM (flux noted ΦM_F) releasing

Table 1. Reactants and products of each process considered by the model and stoichiometry of the reactions. The secondary reactants and products (e.g., H_2O) are not shown. Stoichiometric coefficients are not specified for Ox (oxidative reactions that do not release CO_2) because the contribution of each reactant on the final balance of this process remains unknown. Otherwise, we assume, for instance, that 1 CPOM represents one mole of (carbon + nitrogen) in the CPOM fraction and that 1 CPOC stands for 1 mol of C in the CPOM fraction. The indices (a) and (w) attached to CO_2 and O_2 correspond to air and water, respectively.

Process	Reactants	Products
P_C	CO_2 (w)	CPOM + O_2 (w)
P_F	CO_2 (w)	FPOM + O_2 (w)
V	CO_2 (a)	CPOC
M_C	CPOM	FPOM
M_F	FPOM	DOM
M_D	DOM + O_2 (w)	CO_2 (w)
N	DON	DIN
D	DOM; NO_3^-	5/4 CO_2 (w)
CH_4	DOM	CH_4 (a)
R	CO_2 (w)	CO_2 (a)
O_2	O_2 (w)	O_2 (a)
Ox	NH_4^+; O_2 (w); DOM (HMW)	NO_3^-; NO_2^-; DOM (LMW)
S	DOC	FPOC
S_N	DON	FPON

DOC and DON without consuming O_2; DOM sorption removing DOC (flux noted ΦS) and DON (flux noted ΦS_N) to form POCF and PONF, respectively; aerobic decay of DOC (flux noted ΦM_D) consuming O_2 and releasing DIC; oxidation of DON (flux noted ΦN) consuming O_2 and releasing DIN; methanogenic pathways removing DOM species (flux noted ΦCH_4); denitrification (flux noted ΦD) removing DIN and forming DIC; and the oxidation of inorganic and organic substrates (flux noted ΦOx) consuming O_2 without releasing CO_2. Moreover, the balance of gaseous exchanges between at the air–water interface is controlled by CO_2 outgassing (flux noted ΦR) and by the invasion of O_2 from the atmosphere (flux noted ΦO_2). The deconvolution of processes controlling the chemical (C and N species) and isotopic imbalances is performed by solving the system of linear equations presented in Table 2. To achieve this purpose, several required variables must be established and/or calibrated. The isotopic composition of respired CO_2, noted $\delta^{13}C(R)$, is determined taking into account 1) the chemical fractionation associated to the speciation between HCO_3^- and CO_2, $\delta^{13}C(CO_2) = \delta^{13}C(HCO_3^-) - 8.97$ (Faure 1977) and 2) the physical fractionation associated to the outgassing, $\delta^{13}C(R) = \delta^{13}C(CO_2) - 3.4$ (Craig 1954); 3) the pH-dependent speciation of DIC, $pH = 6.367 + \log[HCO_3^-] - \log[CO_2]$ for $T = 28°C$ [mean temperature of the Amazon River, inferred from the quality survey of the Brazilian Water Agency (ANA)], with $[HCO_3^-] + [CO_2] = [DIC]$, leading to

$$\delta^{13}C(R) = [0.5 \times \delta^{13}C(DIC)_{IN*} + 0.5 \times \delta^{13}C(DIC)_{OUT}] - \frac{1}{1 + 10^{6.367 - pH}} \times 8.97 - 3.4. \quad (4)$$

Table 2. System of linear equations relating 14 river processes to the imbalances of incoming vs. outgoing fluxes relative to carbon and nitrogen species.

$$
\begin{bmatrix} \Delta\Phi(\mathrm{DIC}) \\ \Delta\Phi(\mathrm{DOC}) \\ \Delta\Phi(POCF) \\ \Delta\Phi(\mathrm{POCC}) \\ \Delta(\Phi\mathrm{DIC} \times \delta^{13}\mathrm{CDIC}) \\ \Delta(\Phi POCF \times \delta^{13}\ \mathrm{CPOCF}) \\ \Delta(\Phi\mathrm{POCC} \times \delta^{13}\mathrm{CPOCC}) \\ \Delta\Phi(\mathrm{O_2}) \\ \Delta{\Leftarrow}\Phi\mathcal{DOC} \times \delta^{13}\mathrm{CDOC}) \\ \Delta\Phi(DIN) \\ \Delta\Phi(\mathrm{DON}) \\ \Delta\Phi(\mathrm{PONF}) \end{bmatrix}
+
\begin{bmatrix} \Phi R \\ 0 \\ 0 \\ 0 \\ \Phi R \times \delta^{13}\mathrm{C}(R) \\ 0 \\ 0 \\ \Phi\mathrm{O_2} \\ 0 \\ 0 \\ 0 \\ 0 \end{bmatrix}
=
\begin{bmatrix}
-1 & -1 & 0 & 0 & 0 & 1 & 0 & 0 & 0 & 5/4 & 0 & 0 \\
0 & 0 & -1 & 0 & 1 & -1 & 0 & 0 & -1 & 0 & 0 & 0 \\
0 & 1 & 1 & 1 & -1 & 0 & 0 & 0 & 0 & 0 & 0 & 0 \\
1 & 0 & 0 & -1 & 0 & 0 & 1 & 0 & 0 & 0 & 0 & 0 \\
-\delta^{13}\mathrm{C}(P_C) & -\delta^{13}\mathrm{C}(P_F) & 0 & 0 & 0 & \delta^{13}\mathrm{C}(M_D) & 0 & 0 & 0 & 0 & 0 & 0 \\
0 & \delta^{13}\mathrm{C}(P_F) & \delta^{13}\mathrm{C}(M_S) & \delta^{13}\mathrm{C}(M_C) & -\delta^{13}\mathrm{C}(M_F) & 0 & 0 & 0 & 0 & 0 & 0 & 0 \\
\delta^{13}\mathrm{C}(P_C) & 0 & 0 & -\delta^{13}\mathrm{C}(M_C) & 0 & 0 & \delta^{13}\mathrm{C}(V) & 0 & 0 & 0 & 0 & 0 \\
1 & 1 & 0 & 0 & 0 & -1 & 0 & -1 & 0 & 0 & 0 & 0 \\
0 & 0 & -\delta^{13}\mathrm{C}(M_S) & 0 & \delta^{13}\mathrm{C}(M_F) & -\delta^{13}\mathrm{C}(M_D) & 0 & 0 & -\delta^{13}\mathrm{C}(\mathrm{CH_4}) & 0 & 0 & 0 \\
-\mathrm{N/C}(P_C) & -\mathrm{N/C}(P_F) & 0 & 0 & 0 & 0 & 0 & 0 & 0 & -1 & 0 & 1 \\
0 & 0 & 0 & 0 & \mathrm{N/C}(M_F) & 0 & 0 & 0 & 0 & 0 & -1 & -1 \\
0 & \mathrm{N/C}(P_F) & 0 & \mathrm{N/C}(M_C) & -\mathrm{N/C}(P_F) & 0 & 0 & 0 & 0 & 0 & 1 & 0
\end{bmatrix}
\times
\begin{bmatrix} \Phi P_c \\ \Phi P_F \\ \Phi S \\ \Phi M_C \\ \Phi M_F \\ \Phi M_D \\ \Phi V \\ \Phi\mathrm{O}_x \\ \Phi\mathrm{CH_4} \\ \Phi D \\ \Phi S_N \\ \Phi\mathrm{N} \end{bmatrix}
$$

The flux of respiration (noted ΦR) and the flux of O_2 invasion (noted ΦO_2) are determined at each time step by applying the first Fick's law, in combination with Graham's law,

$$\Phi R_{j,t} = \left\{K_{\mathrm{FP},j} \times (\mathrm{FLA}_{j,t} - \mathrm{MCA}_j) + K_{\mathrm{MC},j} \times \mathrm{MCA}_j\right\} \times \left\{[\mathrm{CO_2}]_{j,t} - 13\right\} \times 10^{-3} \quad \text{and} \tag{5}$$

$$\Phi \mathrm{O}_{2(j,t)} = \sqrt{44/32} \times \left\{K_{\mathrm{FP},j} \times (\mathrm{FLA}_{j,t} - \mathrm{MCA}_j) + K_{\mathrm{MC},j} \times \mathrm{MCA}_j\right\} \times \left\{246 - [\mathrm{O_2}]_{j,t}\right\} \times 10^{-3}, \tag{6}$$

where ΦR and ΦO_2 are given in moles per year, K_{FP} and K_{MC} are bulk gaseous exchange coefficients of the FP and MC expressed in meters per year and calibrated within a constrained search space, $[CO_2]$ and $[O_2]$ are in micromoles per liter, the overall flooded area (FLA; in meters squared) is inferred from remote sensing data (Richey et al. 2002) and successfully related to river discharge (Bustillo 2007), mean channel area (MCA) is in m^2, 13 μmol L^{-1} is $[CO_2]$ saturation level at $T = 28$°C, 246 μmol L^{-1} is $[O_2]$ saturation level at $T = 28$°C, and 10^{-3} is a conversion factor. The subscripts j and t indicate that the considered parameters are spatially (j) and/or temporally (t) variable. The other parameters required to solve the system of linear equations, $\delta^{13}C(P_C)$ and $\delta^{13}C(P_F)$, are the isotopic signatures of POCC and POCF formed by aquatic photosynthesis; $\delta^{13}C(M_C)$, $\delta^{13}C(M_F)$, and $\delta^{13}C(M_D)$ are the isotopic signatures of POCC, POCF, and DOC undergoing physical size reduction or aerobic decay; $\delta^{13}C(M_S)$ designates the isotopic signature of DOC adsorbed onto fine sediments; $\delta^{13}C(V)$ is the isotopic signature of POCC formed by aerial photosynthesis and supplied to the river; $\delta^{13}C(CH_4)$ is the isotopic signature of CH_4 formed by methanogenesis; N/C (P_C) and N/C (P_F) are the N to C atomic ratio of biomass (coarse and fine size fraction, respectively) formed by aquatic photosynthesis; and N/C (M_C) and N/C (M_F) are the N to C atomic ratio of organic matter (coarse and fine size fraction, respectively) submitted to organic decay. These parameters $X^{i,j}$ are calibrated at each sampling station by using linear programming methods (simplex algorithm) under constrained conditions, $X^{i,j}_{\min} \leq X^{i,j} \leq X^{i,j}_{\max}$ (thresholds defined from in-field studies), and by maximizing the performance criterion, Minimum ($\Phi^j_{i,t}$). This criterion was chosen to select, among the pool of possible $X^{i,j}$, the most likely combination for which all calculated $\Phi^j_{i,t}$ are positive, keeping in mind that negative values are physically meaningless.

The optimization process is initiated with the following: $\delta^{13}C(V) = -26‰$ (Victoria et al. 1992); POCC/PONC (V) = 42 (Victoria et al. 1992); $\delta^{13}C$ (P_C) = $\delta^{13}C(P_F) = -33.0‰$ (Martinelli et al. 2003); and $\delta^{13}C(CH_4) = -65.0‰$ (isotopic signature ranging between $-55‰$ and $-75‰$, depending on the nature of dominant methanogenic pathway, according to Moura et al. 2008). The values obtained for each of the calibrated parameters are presented in Table 3. The calibrated values of the gaseous exchange coefficient K (relative to CO_2) at the interface river–atmosphere (160 m yr^{-1} in floodplains versus 610 m yr^{-1} in the main channel) are close to those estimated by Richey et al. (Richey et al. 2002) by means of CO_2 and CH_4 accumulation in free-floating chambers. The contrasts obtained between

Table 3. Calibrated parameters of the process-based model. The parameters were calibrated simultaneously for the seven monitoring stations, by means of linear programming method.

Fraction	DOM		FPOM		CPOM		
parameter	Sorption	Mineralization	Mineralization	Photosynthesis	Mineralization	Photosynthesis	Várzeas
$\delta^{13}C$ (‰)	−33.9	−25.9	−29.1	−31.0	−26.0	−32.1	−25.8
C/N	—	—	14	14	25	42	—

floodplains and main channel are in good agreement with field measures reported by Devol et al. (Devol et al. 1987): $K = 237 \pm 91$ m yr^{-1} in the floodplains versus $K = 840 \pm 91$ m yr^{-1} in the main channel.

4. Results and discussion

4.1. Autotrophy and heterotrophy

4.1.1. Process-based modeling

The specific fluxes relative to photosynthesis and organic matter decay are presented in Figure 3. This indicates that carbon sequestrated by photosynthesis ($\Phi P = \Phi P_F + \Phi P_C + \Phi V$) is balanced by the flux of mineralization (ΦM_D). On average, the specific fluxes of photosynthesis and organic matter decay are 1054 g C m^{-2} yr^{-1}. This is consistent with the field studies of Wissmar et al. (Wissmar et al. 1981) and Quay et al. (Quay et al. 1995) that report depth-integrated gross photosynthesis rates as high as 160 mmol C m^{-2} day^{-1} = 700 g C m^{-2} yr^{-1}. It represents 50% of the carbon flux (all chemical species compounded) transported by the river. Almost 57% of the carbon sequestrated by photosynthesis comes from aerial sources (noted ΦV), with the remaining 43% resulting from aquatic sources (noted $\Phi P_F + \Phi P_C$). The aerial sources refer implicitly to the aquatic grasses whose net primary productivity (NPP) reaches locally 4000 g C m^{-2} yr^{-1} (Piedade et al. 1991). Moreover, it must be emphasized that the proportion of organic matter formed by aquatic photosynthesis ($1 - \Phi V/\Phi P$) increases during lowest waters (Figure 3), when the sunlight penetration and the water limpidity are at their maximum. Conversely, this proportion decreases to the benefit of aerial sources (i.e., aquatic grasses mainly) during falling water stage, precisely when the direction of river–floodplain discharge is orientated toward the main channel. The differences between sampling stations are moderate: ΦM_D ranges between 784 g C m^{-2} yr^{-1} at Paura (Pau) and 1117 g C m^{-2} yr^{-1} at Jutica (Jut). It is higher but within the order of magnitude of respiration rates reported locally by Benner et al. (Benner et al. 1995) for CAMREX 11, 12, and 13 (average = 0.61 ± 0.17 μM O_2 h^{-1} ⇔ 538 ± 150 g C m^{-2} yr^{-1} over 34 000 km^2 for a residence time of 20 days) and by Devol et al. (Devol et al. 1995) reporting the pluriannual time series of Marchantaria, close to Manacapurú (Man; average = 0.53 ± 0.11 μM O_2 h^{-1}, $n = 44$; maximum = 1.73 μM O_2 h^{-1}). The seasonal contrasts are limited: greatest specific fluxes observed during lowest waters, supporting the idea that photochemical processes (favored in unshaded main channels) could transform refractory DOM to more labile substrates that are readily utilized by heterotrophic bacteria (Amon and Benner 1996).

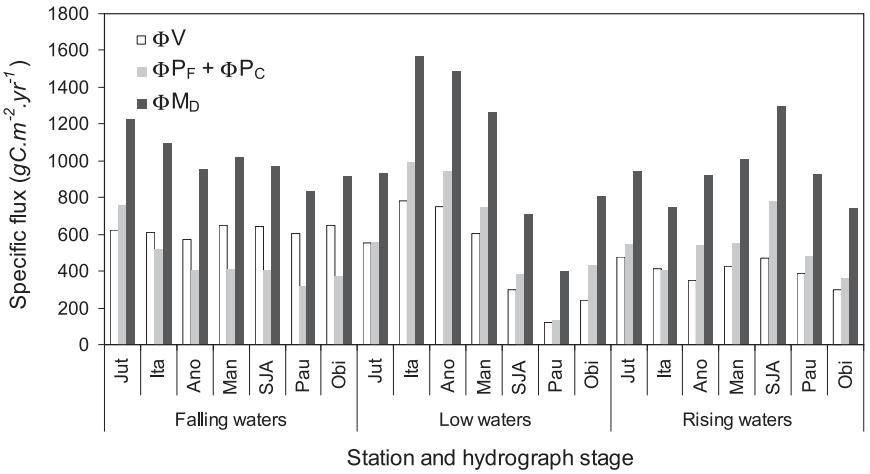

Figure 3. Specific flux of carbon (expressed in g C m^{-2} yr^{-1}) associated to organic matter decay (ΦM_D) and photosynthesis (with a distinction between aquatic photosynthesis $\Phi P = \Phi P_F + \Phi P_C$ and aerial photosyntheses ΦV) for three distinct hydrograph stages (falling waters: average of cruises 2, 5, and 8; low waters: average of cruises 3 and 6; rising waters: average of cruises 4 and 7) at seven sampling stations: Jut, Ita, Ano, Man, SJA, Pau, and Óbi (the outlet of the studied reach). Data correspond to specific fluxes between the upstream boundary (VG) and each considered station, estimated by constraining the chemical and isotopic budgets of carbon and nitrogen.

4.1.2. Factors influencing hydrobiological equilibria

The gaseous composition of the Amazon River (O_2, CO_2) constitutes a very insightful marker of hydrobiological processes occurring in the main channel and in floodplains. Depending on if the hydrobiological regime is dominantly autotrophic or heterotrophic, the effects on the chemistry of the river water differ substantially (Bustillo et al. 2010). These processes do not modify fundamentally the chemical baseline measured in the inflow, but they imprint the chemical composition of river water on several parameters. As mentioned previously by Bustillo et al. (Bustillo et al. 2010) and based on the outcomes of the end-member mixing models, the nature and magnitude of hydrobiological paths are intrinsically related to the hydrograph stage via the turbidity of water, the direction of water circulation between the main channel and adjacent floodplains, the time of residence of water in submerged areas, and the bioavailability of organic carbon. As the river level rises, the light attenuation due to the turbidity of water limits the rate of photosynthesis (Fisher 1979). Concomitantly, the surface runoff transports large amounts of organic carbon whose bioavailability is expected to be greater than the bulk of riverine materials. The supply of labile organic substrate is the main limiting factor of heterotrophic metabolism in the Amazon River (Benner et al. 1995). The mineralization is very active in floodplains, where the flow velocity is lower than in the main channel and where the time of residence is greater. The aquatic

grasses growing in floodplains remove CO_2 and nutrients (N, P, K, Ca, and Mg) and release O_2 in the river water, but the rate of photosynthesis remains much lower than the rate of mineralization at the annual scale. As the floodplains dry up, the heterotrophic regime of floodplains is made manifest by the discharge of floodplains toward the main channel. The autochthonous organic matter, formed by photosynthesis and exhibiting heavy isotopic signature ($\delta^{13}C = -12 \pm 2‰$, related to C_4 photosynthetical pathway of aquatic grasses), is preferentially released at this stage. The isotopic signature is very ^{13}C enriched compared to wood ($\delta^{13}C = -28 \pm 1‰$) and leaf ($\delta^{13}C = -30 \pm 1‰$) material from 15 of the most abundant tree species in the igapo, várzea, and terra firme forests of the lowland Amazon basin (Hedges et al. 1986a). During the second stage of falling waters, with the turbidity of waters and the bioavailability of organic carbon being much lower, an inversion of the hydrobiological regime arises (mineralization → aquatic photosynthesis) and even accentuates as the river flow decreases. The dominance of photosynthesis over mineralization leads to a rapid decrease of $[CO_2]$ and to a concomitant increase of $[O_2]$ that nearly reaches the level of saturation (246 μmol L^{-1} at $T = 28°C$). These rapid variations lead principally to the rise of pH and $\delta^{13}C$ (DIC), the latter being interpreted as the result of the preferential uptake of ^{13}C-depleted CO_2 by aquatic plants. This isotopic pattern with respect to DIC was reported by several authors in different climatic conditions: temperate zone (Lagan River: Barth et al. 2003; Tyne and Tweed: Ahad et al. 2008; Rhône: Aucour et al. 1999), subtropical zone (Patagonian rivers: Brunet et al. 2005), equatorial zone (Orinoco: Tan and Edmond 1993), and subboreal zone (St. Lawrence: Barth and Veizer 1999; Fraser: Cameron et al. 1995). On average, the ^{13}C enrichment of DIC can be explained by the decreasing influence of carbonate dissolution on the chemical erosion balance of carbon as we move downstream. This topic was extensively documented by Tardy et al. (Tardy et al. 2005; Tardy et al. 2009) and Bustillo et al. (Bustillo et al. 2010) by means of interbasin analysis, with ^{13}C-enriched signal impulsed by upstream areas (Solimões River: $-13 \pm 2‰$) and ^{13}C-depleted signals in downstream tributaries (e.g., Negro River: $-27 \pm 2‰$) draining crystalline rocks.

4.2. Diagenesis of dissolved organic matter

4.2.1. Preliminary observations

The temporal variations of $[NO_3^-]$, pH, $[O_2]$, [DON], and [DOC]/[DON] exhibit between-station similarities, which can be understood as the result of the DOM diagenesis leading to mineralization, sorption, and condensation. The inputs by the small ungauged black rivers are probably significant, unlike those of sediments, for instance. It is even highly probable that the concentrations of DOM in the small rivers draining lowlands are higher than in the Amazon main channel. The samples collected in the river Trombetas during the HiBAm project (Moreira-Turcq et al. 2003a) show that [DOC] fluctuates between 1.6 and 11.2 mg C L^{-1} (weighed average = 6.5 mg C L^{-1}) confirming thus that small ungauged tributaries are significant providers of DOM. Hence, the apparent stability of [DOM] might mask very significant diagenetic processes.

Chemical analyses performed on DOM molecules (dissolved humic substances: Ertel et al. 1986; carbohydrates and amino acids: Hedges et al. 1986a; Hedges et al.

Table 4a. Balance of humic substances (mass balance given in kg C s^{-1}, from Ertel et al. 1986), discriminating HA and FA. Comparison is between observed fluxes and expected (calculated) fluxes.

	HA		FA		FA/HA		FA + HA	
	Obs	Calc	Obs	Calc	Obs	Calc	Obs	Calc
VG	9.9	9.9	55.8	55.8	5.66	5.66	65.7	65.7
Xib	11.1	11.7	65.2	64.2	5.87	5.47	76.3	75.9
Tup	13.8	15.6	75.0	73.2	5.43	4.68	88.8	88.8
Jut	22.0	23.9	103.0	100.1	4.68	4.19	125.0	123.9
Ita	23.9	23.9	88.9	100.1	3.72	4.19	112.8	123.9
Man	25.3	31.0	130.0	116.8	5.14	3.77	155.3	147.8
SJA	77.3	94.9	225.0	215.1	2.91	2.27	302.3	310.3
Pau	73.1	102.5	239.0	262.9	3.27	2.57	312.1	365.3
Óbi	64.1	102.5	219.0	262.9	3.42	2.57	283.1	365.3

1994) and $\Delta^{14}C$ ages (Hedges et al. 1986b) provide, to this effect, insightful information. According to Ertel et al. (Ertel et al. 1986), humic substances represent 60% of the riverine DOM with fulvic to humic acid (FA/HA) ratios in the main stem averaging 4.7. Compared mass transfer balances (Table 4a) indicate significant losses of humic acids after the confluence of Rio Negro (Manacapurú–Óbidos reach) as a result of HA adsorption onto fine particles, which constitute the bulk of available surface area. This is confirmed by adsorption experiments performed by Moreira-Turcq et al. (Moreira-Turcq et al. 2003b) using dissolved and particulate materials from the mixing zone of the Rio Negro and Rio Solimões. Higher N/C and higher O/C in the fulvic fraction (Table 4b) and lower O/C and higher N/C in the fulvic fraction (Table 4c) indicate that adsorption processes affect preferentially the more hydrophobic humic acids (Leenheer 1980). The H/C ratio observed for the Rio Negro humic acids (0.79) reveals a strong hydrophobicity, which probably encourages its preferential sorption on suspended sediments conveyed by the Amazon River main stem (Tardy et al. 2009). The active sorption of the most hydrophobic fraction of humic acids, originating from Rio Negro, leads to a

Table 4b. Mean elemental composition of HA (calculated from Ertel et al. 1986), for C = 100. Comparison is between observed composition and expected (calculated) composition.

	HA (obs)				HA (calc)			
	C	H	O	N	C	H	O	N
VG	100	110.0	61.1	6.02	100	110.0	61.1	6.02
Xib	100	110.0	61.7	6.71	100	110.0	61.7	5.93
Tup	100	110.0	64.8	6.54	100	106.8	60.6	5.63
Jut	100	92.0	66.9	4.81	100	102.2	62.4	5.27
Ita	100	94.0	73.2	3.65	100	102.2	62.4	5.27
Man	100	100.0	72.2	5.10	100	101.7	63.1	5.05
SJA	100	83.0	61.8	2.60	100	86.4	62.9	2.81
Pau	100	87.0	64.3	3.36	100	87.1	63.3	2.92
Óbi	100	90.0	69.9	3.31	100	87.1	63.3	2.92

Table 4c. Mean elemental composition of FA (calculated from Ertel et al. 1986), for C = 100. Comparison is between observed composition and expected (calculated) composition.

	FA (obs)				FA (calc)			
	C	H	O	N	C	H	O	N
VG	100	100.0	87.0	1.63	100	100.0	87.0	1.63
Xib	100	96.0	66.9	1.68	100	99.5	86.1	1.62
Tup	100	99.0	67.5	1.89	100	98.8	85.3	1.57
Jut	100	98.0	63.3	1.65	100	98.1	80.3	1.57
Ita	100	94.0	61.8	1.43	100	98.1	80.3	1.57
Man	100	110.0	64.0	2.01	100	98.2	78.1	1.60
SJA	100	96.0	60.8	1.54	100	96.8	70.7	1.41
Pau	100	100.0	61.3	1.63	100	97.4	69.0	1.57
Óbi	100	100.0	63.2	1.67	100	97.4	69.0	1.57

transfer of carbon from the dissolved compartment to the mineral-associated compartment (POCF). Because of their hydrophobicity and aromaticity, the humic acids tend to be ^{13}C depleted (Tardy et al. 2009), leading thus to the ^{13}C depletion of the POCF fraction when river pH decreases (Bustillo et al. 2010).

4.2.2. Process-based modeling

The yield of DOM sorption, estimated by ΦS/Qt and ΦS_N/Qt (Qt is river flow) and expressed in μM, was established by constraining the chemical and isotopic budgets of carbon, oxygen, and nitrogen species. The results obtained at seven sampling stations are presented in Figure 4a. The mean yield of DOC sorption is 114 μM and represents more than 25% of incoming [DOC] in the Amazon River, whereas the yield of DON sorption averages 19 μM: that is, as much as the incoming [DON]. This indicates that the C/N molar ratio of adsorbed DOM averages 7, close to that of proteins (6.25). It is much lower than DOC/DON in the river water, averaging 30. The variations between sampling stations are limited; the striking fact is the distinct response depending if we consider falling water stage (cruises 2, 5, and 8) for which sorption rate is high compared to rising water stage (cruises 4 and 7) and low water stage (cruises 3 and 6). It indicates that DOM formed in the floodplains by organic decay (autochthonous source) tends to be adsorbed onto suspended matter, removing it from the pool of labile compounds. Samples collected during low water and rising water stages might occasionally exhibit higher $\Phi S/\Phi S_N$, supporting the idea that allochthonous soil-derived DOM coming with surface runoff and undergoing sorption processes has higher C/N (e.g., humic acids).

Another important issue to analyze resides in the comparison of DOC mineralization (noted ΦM_D) versus DON mineralization (noted ΦN). The results are represented in Figure 4b. On average, $\Phi M_D/\Phi\text{N} = 16$. It means that 16 mol of organic carbon are mineralized for each mole of organic nitrogen. It is much lower than the molar ratio C/N of dissolved organic matter transiting in the Amazon River, ranging between 20 and 70 (average = 30; Tardy et al. 2009). This indicates that the nature of DOM that fuels mineralization (low C/N) differs from the bulk of DOM transiting in the river, which is more refractory. Actually, autochthonous organic sources derived from aquatic photosynthesis provide low C/N molecules.

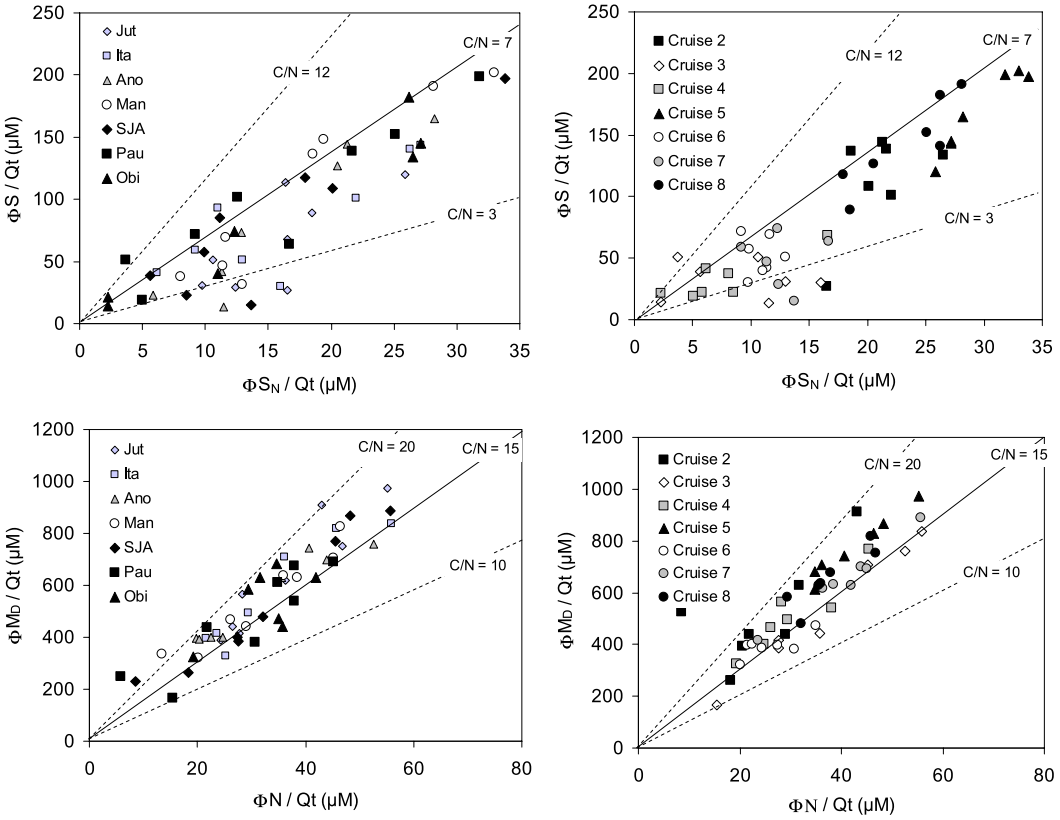

Figure 4. Relationships between (a) the sorption yield of carbon (ΦS/Qt; μM) and the sorption yield of nitrogen (ΦS_N/Qt; μM) and (b) the mineralization rate of DOC (ΦM_D/Qt; μM) and the mineralization rate of DON (ΦN/Qt; μM) for the seven considered sampling stations: Jut, Ita, Ano, Man, SJA, Pau, and Óbi (the outlet of the studied reach).

In well oxygenated waters and unshaded environments, these low C/N molecules undergo mineralization and photochemical reactions that release end products of reaction: that is, CO_2 and NO_3^-. The organic nitrogen is preferentially removed, compared to organic carbon, and this leads to the formation of high C/N molecules, as in cruises 2 (upstream from Negro confluence), 3 (downstream from Negro confluence), and 6 for which DOC/DON exceeds 50. The DOC exhibits a conservative behavior unlike DON, which probably constitutes a preferential substrate for oxidation processes, which involves more particularly photochemical ammonification that leads to the formation of a variety of low molecular weight organic compounds (Amon and Benner 1996) and finally to the release of DIN (Bushaw et al. 1996).

4.2.3. Insights from thermodynamics

In light of inverse evolution between DON, on the one hand, and NO_3^- and O_2, on the other (Bustillo et al. 2010), it can be hypothesized that the invasion of dissolved O_2 in the river water controls the dynamics of nitrogen and the relative proportions

of DON and NO_3^-. The side-chain oxidation of humic substances determining a release of NO_3^- in river water and a rise of DOC/DON molar ratio may be formalized as follows:

$$C_{x1}H_{y1}O_{z1}N_{t1}^{n1-} + \alpha O_2 \rightarrow C_{x2}H_{y2}O_{z2}N_{t2}^{n2-} + (t1 - t2)NO_3^- + \beta CO_2 + \gamma H_2O, \tag{7}$$

where $n1/x1$ = ionic charge [given in eq (mol C)$^{-1}$] of low C/N (DOM); $n2/x2$ = ionic charge of high C/N (DOM); $x1$, $y1$, $z1$, and $t1$ = elemental composition of organic reactant (C, H, O, and N for low C/N molecule, respectively); $x2$, $y2$, $z2$, and $t2$ = elemental composition of organic product (high C/N molecule); and α, β, and γ = stoichiometric coefficients of O_2, CO_2, and H_2O. The reaction constant (Kr) is as follows:

$$\log Kr = (t1 - t2)\log[NO_3^-] + \log[C_{x2}H_{y2}O_{z2}N_{t2}^{n2-}] - \log[C_{x1}H_{y1}O_{z1}N_{t1}^{n1-}] + \beta \log[CO_2] - \alpha \log[O_2], \tag{8}$$

assuming $[H_2O] = 1$. The calibration of Equation (8) for the Óbidos station yields $\alpha = 17.46$ and $\beta = 5.30$. We assume conventionally that reactant and product display [DOC]/[DON] = 10 and [DOC]/[DON] = 75 and a mean ionic charge of DOM equivalent to $n = 5.35$ μeq mg C^{-1} (microequivalent milligrams of carbon) [0.064 eq (mol C)$^{-1}$; equivalent moles of carbon], as proposed by Tardy et al. (Tardy et al. 2005). For $t1 - t2 = 8$ and according to the characteristic molar ratios of the humic substances, thus we get

$$C_{91.5}H_{91.5}O_{54.9}N_{9.15}^{5.85-} + 17.46\ O_2 \rightarrow C_{86.2}H_{86.2}O_{52.6}N_{1.15}^{1.26-} + 8\ NO_3^- + 5.3\ CO_2 + 2.65\ H_2O, \tag{9}$$

with logKr = +6.69 (Figure 5).

The variations of $[NO_3^-]$ and [DOC]/[DON] are controlled by the differences of $[CO_2]$ (or pH) and $[O_2]$ in the river, as a consequence of 1) the hydrological source contributions, 2) the geographical repartition of drainage, and 3) hydrobiological processes (aquatic photosynthesis versus organic decay). Reaction kinetics is slow compared to hydrobiological processes; as a result, the seasonal fluctuations of $[CO_2]$ and $[O_2]$ are poorly influenced by DOM diagenesis. Therefore, the fulfillment of equilibria conditions implies that $[NO_3^-]$ and [DOM] (low C/N fraction) evolve symmetrically.

The oxidation of DOM in the river water is a plausible explanation of seasonal and longitudinal (spatial) compositional variations of $[NO_3^-]$ and [DOC]/[DON]. The thermodynamic approach enables us to predict the dynamics of nitrogen in the river as a function of the two driving factors, which are $[CO_2]$ and $[O_2]$. The results presented (Table 5) are established from

$$\log Kr = 8 \times \log[NO_{3\_}] + \log[P/R] + 5.3 \log[CO_2] - 17.46 \times \log[O_2] = 6.69. \tag{10}$$

The initial conditions (for pH = 6.60) are determined in such a way that values are compatible with Kr and with observed concentrations in the Amazon River at

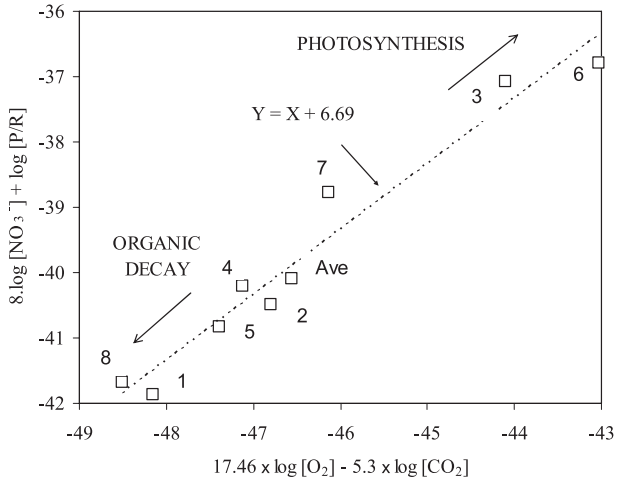

Figure 5. Calibration of equilibrium constant (Kr) and stoichiometric coefficients (α and β) concerning the reaction of DOC polymerization, involving O_2, CO_2, NO_3^-, organic reactant R ($C_{91.5}H_{91.5}O_{54.9}N_{9.15}^{5.85-}$), and organic product P ($C_{86.2}H_{86.2}O_{52.6}N_{1.15}^{1.26-}$) for the Amazon River at the station of Óbi.

Óbidos, leading to $[NO_3^-]_{pH=6.6} = 7.01$ and $[DOC]/[DON]_{pH=6.6} = 16.0$. The atomic ratio [DOC]/[DON] is calculated as follows:

$$[DOC]/[DON] = (75 \times P/R + 10)/(1 + P/R), \quad (11)$$

with P/R corresponding to the molar ratio between organic product ($C_{91.5}H_{91.5}O_{54.9}N_{9.15}^{5.85-}$) and organic reactant ($C_{86.2}H_{86.2}O_{52.6}N_{1.15}^{1.26-}$). The modeled variations of [DOC]/[DON] and $[NO_3^-]$ are in very good agreement with those measured in the Amazon River (Figure 6). The large amounts of dissolved O_2 involved in the reaction lead to the release of CO_2 and NO_3^-, end products of the oxidative reactions.

4.2.4. Concluding remarks

The scheme presented above, resulting from thermodynamic and process-based modeling, is consistent with the paradigm promoted by Hedges et al. (Hedges et al. 1994), Aufdenkampe et al. (Aufdenkampe et al. 2001), and Aufdenkampe (Aufdenkampe 2002). According to these authors, the side-chain oxidation of fresh organic materials tends to release nitrogenous species, where the adsorption by clays forms the mineral-associated fraction POCF. The hydrolysable amino acids and the carbohydrates represent approximately 3.2% and 2.8% of the total DOC and appear to be significantly underrepresented compared to the mineral-associated fraction (POCF; 31.9% and 10.7%, respectively) and coarse fraction (POCC; 12.9% and 16.4%, respectively). The distribution of amino acids is very homogeneous within each size fraction but highly variable from fraction to fraction. The basic amino acids (glutamine, arginine, and asparagine) exhibiting positively

Table 5. Expected evolution of NO_3^-, DOC-1 (low C/N), DOC-2 (polymer, high C/N), and C/N (DOC) as a function of pH and O_2 for the station of Óbi.

	μmol L^{-1}			Molar ratio		
pH	O_2	CO_2	NO_3	P/R	C/N (DOC)	LogKr
6.60	125	235	7.01	0.10	16.0	6.69
6.67	132	220	7.93	0.14	18.0	6.69
6.73	139	205	8.90	0.20	20.8	6.69
6.80	146	190	9.94	0.29	24.6	6.69
6.86	153	175	11.05	0.44	29.8	6.69
6.93	160	160	12.21	0.69	36.5	6.69
6.99	167	145	13.45	1.14	44.6	6.69
7.06	174	130	14.74	2.0	53.2	6.69
7.12	181	115	16.11	3.7	61.3	6.69
7.19	188	100	17.54	7.7	67.5	6.69
7.25	195	85	19.04	17.8	71.5	6.69

charged nitrogen side chains are preferentially adsorbed, as confirmed by in vitro experiments performed by Aufdenkampe (Aufdenkampe 2002). The dissolved organic substances leached from soils and released in rivers are constituted by an aromatic nucleus (mainly hydrophobic and ^{13}C depleted) and N-enriched side chains (^{13}C enriched), resulting of phenol-amine condensation (Stevenson 1994). These side chains might be preferentially oxidized in the river water, released under the form of labile amino acids and partly adsorbed on suspended sediments. Unsorbed fraction of amino acids may therefore undergo rapid degradation, as suggested by their low representation in the DOM fraction, and this releases high quantity of NH_4^+, subsequently oxidized into NO_3^- in presence of O_2.

4.3. Budget of gases in the floodplains

4.3.1. Preliminary observations

The mixing models implemented by Bustillo et al. (Bustillo et al. 2010) indicate that the seasonal fluctuations of [CO_2] and [O_2] are closely related to the variations of the river–floodplain connectivity. The greatest [CO_2] contents coincide with the maximum extension of submerged areas. It is likely that the input of CO_2 results from the decay of organic matter deposited together with sediments or retroceded by the riparian vegetation (grass várzeas and trees). When the extension of floodplains is the smallest, a part of the CO_2 released by organic matter decay is evacuated with the baseflow but the major fraction is released to the atmosphere, causing a fractionation of DIC and a subsequent increase of $^{13}C/^{12}C$ in the river water. The increase of $\delta^{13}C$ (DIC) involves not only the soil respiration of CO_2 but also the aquatic photosynthesis. When the extension of floodplains is at maximum, CO_2 outgassing is high in such a way that CO_2 concentration rises strongly while $\delta^{13}C$(DIC) decreases drastically, compared to the inflow.

An important observation is illustrated in Figure 7, showing an inverse relationship between [DIC] and $\delta^{13}C$(DIC) shifts for the Óbidos station. The excess of DIC (cruises 1, 2, and 8) coincides with the more negative $\delta^{13}C$ (DIC) values, indicating that additional DIC is more ^{13}C depleted than incoming DIC. This is

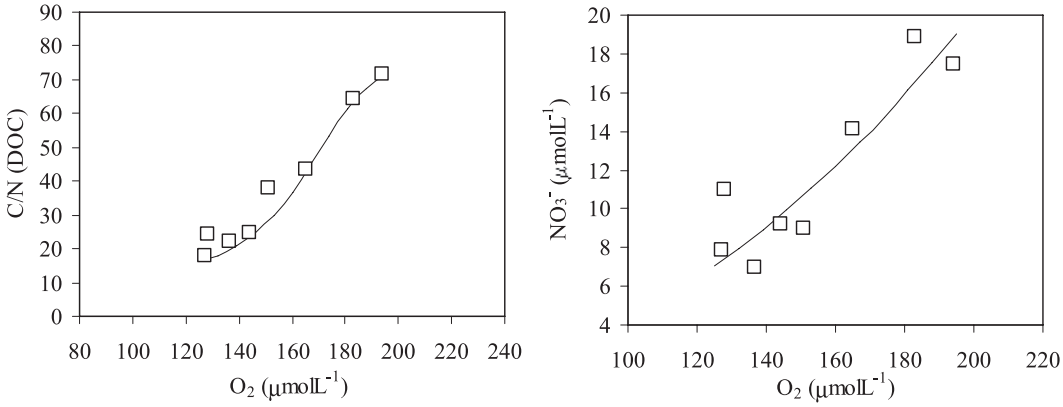

Figure 6. Variation of (DOC)/(DON) and (NO_3^-) as a function of (O_2). Comparison between the observed values (squares) at the station of Óbi and the simulated values (solid line).

consistent with the observations of Ahad et al. (Ahad et al. 2008) concerning two English rivers exhibiting seasonalized δ^{13}C(DIC) signals in relation with seasonalized biogeochemical patterns. Conversely, when the balance of DIC is deficient (Δ[DIC] < 0), the isotopic shift is more attenuated (cruises 3–5), indicating that the loss of DIC (via outgassing or photosynthesis) compensate, at least in part, to the lightening associated to the additional source. This is consistent, for instance, with the observations of Brunet et al. (Brunet et al. 2005) on Patagonian rivers and Barth and Veizer (Barth and Veizer 1999) on the St. Lawrence River, mentioning ^{13}C-enriched DIC signals (δ^{13}C temporally > 0) related to isotopic fractionation by outgassing over extended water bodies (estuaries, lakes). The downstream increasing trends with respect to δ^{13}C(DIC) reported by Doctor et al. (Doctor et al. 2008) at the Sleepers River Research Watershed (Vermont) indicate that CO_2 outgassing influences δ^{13}C(DIC) signals, even for very small streams. Following

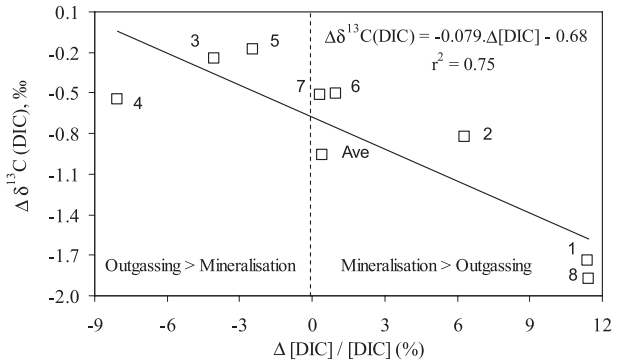

Figure 7. Inverse relationship between the default of (DIC) concentration and the deviation of δ^{13}C(DIC) values for the station of Óbi. View of source and sink relative to dissolved inorganic carbon.

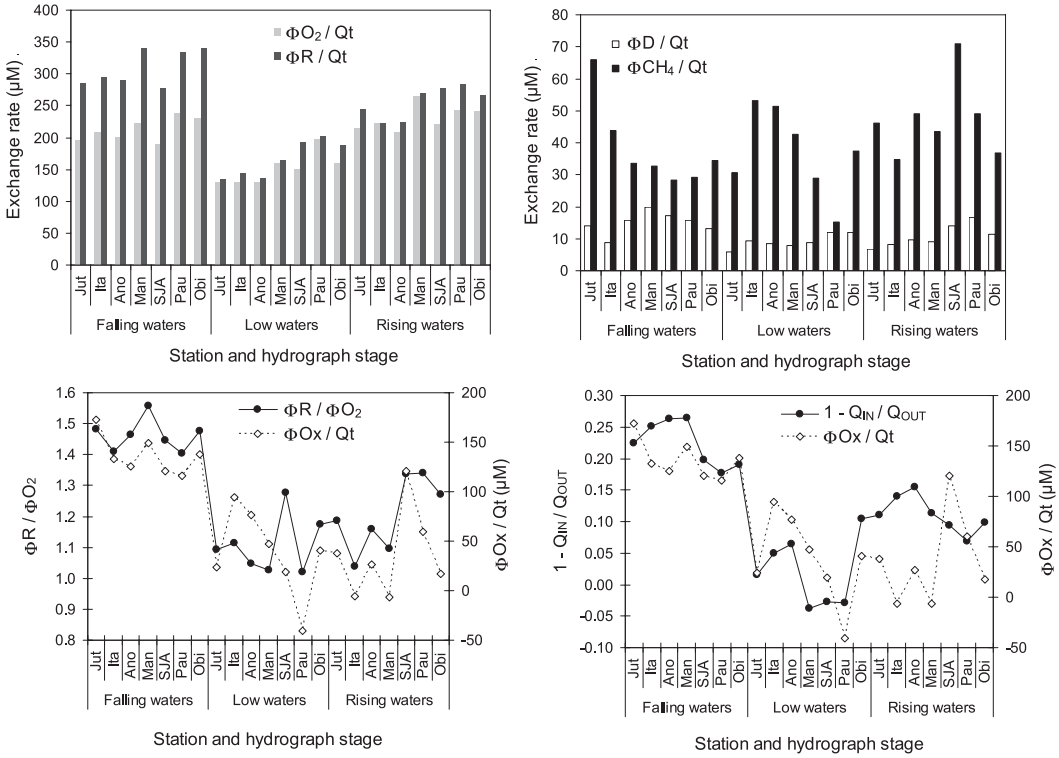

Figure 8. Invasion rate of O_2 (ΦO_2/Qt; μM); outgassing rates of CO_2 (ΦR/Qt; μM), CH_4 (ΦCH_4/Q; μM) ,and N_2 (ΦD/Qt; μM); and oxidation rate of noncarbonaceous functional groups (ΦOx/Qt; μM) for three distinct hydrograph stages (falling waters: average of cruises 2, 5, and 8; low waters: average of cruises 3 and 6; rising waters: average of cruises 4 and 7) at seven sampling stations: Jut, Ita, Ano, Man, SJA, Pau, and Óbi (the outlet of the studied reach).

Richey et al. (Richey et al. 2002), we state that CO_2 outgassing over the studied Amazon reach releases large amounts of CO_2 toward the atmosphere and that organic matter decay arising in aquatic environments provides it.

4.3.2. Process-based modeling

According to our calculations based on the closure of chemical and isotopic budgets, the rate of O_2 invasion (ΦO_2/Qt, expressed in μM) and the rate of CO_2 evasion (ΦR/Qt; μM) tend to balance each other (Figure 8a), except during the falling water stage where $\Phi R/\text{Qt} > \Phi O_2/\text{Qt}$. On average, these rates reach 280 μM, representing $280/1000 = 28\%$ of the carbon (all chemical species confounded) transported at the outlet of Óbidos, and they correspond to a flux of CO_2 outgassing toward the atmosphere of 1567×10^9 mol yr^{-1} over the reach Vargem Grande–Óbidos. The rate of methane emission ranges between 29 and 48 μM depending on the station; it represents about 10%–15% of the rate of CO_2 respired. This proportion is in good agreement with previous estimations from Richey et al. (Richey et al. 1988). The rate of denitrification (ΦN/Qt) ranges between 10 [Itapeua (Ita)] and

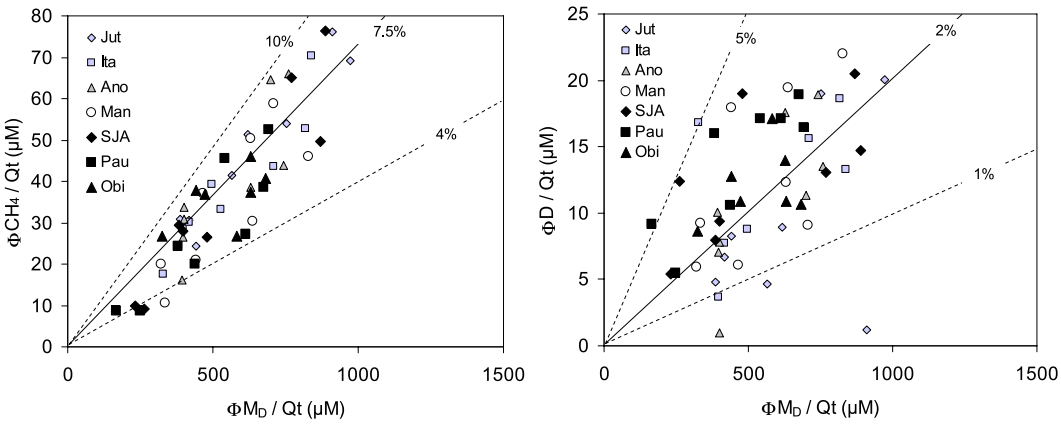

Figure 9. Relationships between the outgassing rates of CH_4 ($\Phi CH_4/Qt$; μM) and N_2 ($\Phi D/Qt$; μM) and the mineralization rate of DOM ($\Phi M_D/Qt$; μM) for the eight cruises of the CAMREX project at seven sampling stations: Jut, Ita, Ano, Man, SJA, Pau, and Óbi (the outlet of the studied reach).

14 μM (Manacapurú); at Óbidos, the rate of denitrification is evaluated to 12 μM, corresponding to 151 kg N ha^{-1} yr^{-1} if considering that the floodplain covers an area of 60 000 km^2. It represents a flux equivalent to 0.87×10^9 kg N yr^{-1}: that is, 1.5 times the flux of DIN exported by the Amazon River at the Óbidos station (0.64×10^9 kg N yr^{-1}). It is in good agreement with values obtained by Salati et al. (Salati et al. 1982) on fertile várzea soils in Central Amazonia (200 kg N ha^{-1} yr^{-1}). For each sampling station, the seasonal variations of ΦD and ΦCH_4 are intrinsically related to the rate of mineralization ΦM_D (Figure 9). High rates of mineralization promote high rates of denitrification and methane emission. It is confirmed by in-field measures performed by Devol et al. (Devol et al. 1988), with the highest rate of CH_4 emission over water surfaces covered by highly productive aquatic macrophytes (590 mg CH_4 m^{-2} day^{-1}) versus 110–120 mg CH_4 m^{-2} day^{-1} over flooded forests and open lake areas. The overall average rate of CH_4 emission from wetlands was 390 mg CH_4 m^{-2} day^{-1} representing 5.77 Tg C yr^{-1} if extrapolated to the whole submerged area at the time of sampling (54 000 km^2) and only 3.63 Tg C yr^{-1} if extrapolated to the mean annual submerged area (34 000 km^2). It is consistent with the mean annual rate of methane emission calculated by the process-based model: 2.18 Tg C yr^{-1}. The rate of oxidation ($\Phi Ox/Qt$; μM) relative to noncarbonaceous functional groups averages 75 μM, all stations gathered. It is a very significant sink of O_2, whose spatial and temporal variations are very well correlated to $\Phi R/\Phi O_2$ ($r = 0.85$) and to the hydrological contribution of local sources ($r = 0.80$; see Figure 8). Actually, high rates of mineralization arising in the floodplains provide considerable amount of low C/N molecules, highly labile whose functional groups are readily oxidized. This process accounts for the removal of O_2 without release of CO_2, occurring especially in highly productive areas bordering the river main channel. This process sustains the undersaturation of O_2 in the river water with respect to the atmosphere.

Table 6. Mean rates of reactions (data given in μM; cruises 1–8) calculated by the process-based model on the seven selected sampling stations located along the Amazon River: Jut, Ita, Ano, Man, SJA, Pau, and Óbi. Shown are the following: ΦP_C (aquatic photosynthesis forming coarse organic matter; >63 μm); ΦP_F (aquatic photosynthesis forming fine organic matter; 0.45–63 μm); ΦV (supply of autochthonous organic matter formed by aerial photosynthesis (CO_2 picked up in the atmosphere and O_2 released to the atmosphere) in the várzeas); ΦM_C (physical and biologically mediated processes leading to the size reduction of the coarse organic matter into fine organic matter); ΦM_F (physical and biologically mediated processes leading to the size reduction of the fine organic matter into DOM); ΦM_D (biologically mediated mineralization of DOM forming DIC); ΦN (oxidation of dissolved organic nitrogen (biologically mediated and photochemical ammonification) forming DIN); processes leading to the release of greenhouse gases to the atmosphere (in hypoxic or anoxic environments (denitrification: ΦN; methanogenesis: ΦCH_4) and CO_2 outgassing (ΦR)); ΦO_2 (invasion of O_2 from the atmosphere); ΦOx (oxidation of DOM (DOC and DON) and dissolved inorganic matter (DIN) that remove O_2 without releasing CO_2); ΦS (sorption of DOC onto fine sediments to form FPOC); and ΦS_N (sorption of DON onto fine sediments to form FPON).

Process	Jut	Ita	Ano	Man	SJA	Pau	Obi
ΦP_C/Qt	23	23	18	19	17	17	21
ΦP_F/Qt	344	272	268	231	238	175	225
ΦS/Qt	70	86	76	118	89	106	114
ΦM_C/Qt	347	330	303	334	295	301	354
ΦM_F/Qt	754	677	641	695	632	573	668
ΦM_D/Qt	648	573	558	553	527	485	572
ΦV/Qt	329	314	285	312	276	279	327
ΦOx/Qt	88	75	81	85	92	69	103
ΦCH_4/Qt	48	40	40	34	35	29	35
ΦD/Qt	10	10	11	14	13	14	12
ΦS_N/Qt	16	17	15	19	16	17	19
ΦN/Qt	37	31	33	32	32	28	32
ΦR/Qt	244	244	242	297	262	296	301
ΦO_2/Qt	188	193	185	216	184	223	219

4.4. Overview of C and N biogeochemical cycles in the floodplains

The process-based methodology based on the balance of chemical and isotopic budgets of carbon and nitrogen species provides an insightful overview of the biogeodynamics relative to C and N over the studied 2000-km reach. The mean results (cruises 1–8) obtained for the seven stations are presented in Table 6. Because of the close similarity of the outcomes for the seven stations, the case of the station of Óbidos is more particularly discussed, and it is sketched in Figure 10.

Over the 2000-km reach between Vargem Grande and Óbidos, the rate of CO_2 outgassing is 1.567×10^{12} mol yr^{-1}, corresponding to a concentration of about 301 μmol L^{-1}. This represents 50% of the rate of export of DIC at the outlet of the studied reach. A significant part of CO_2 is removed by the aquatic photosynthesis (1.284×10^{12} mol yr^{-1}) whose flux corresponds to 43% of the flux of mineralization, estimated to be 2.979×10^{12} mol yr^{-1}. It corresponds roughly to the $\Phi P/\Phi M$ ratio given by Cole et al. (Cole et al. 1994) for the Amazon River (0.33). The invasion

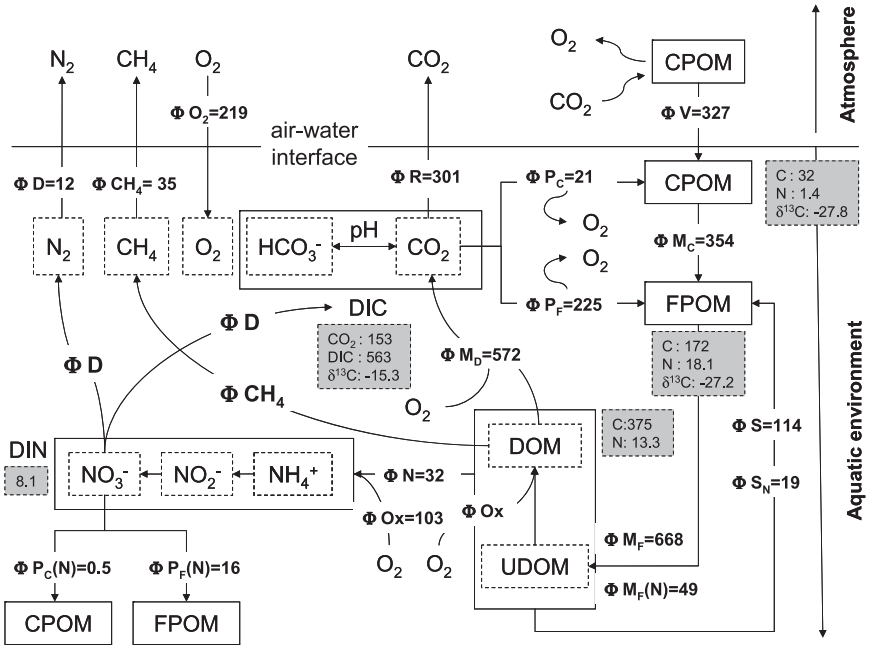

Figure 10. Overview of major processes driving C and N biogeodynamics on the VG–Óbi reach of the Amazon River. Results of the calculations are based on the balance of chemical and isotopic budgets by means of process-based modeling.

of O_2, although of high magnitude (1.142×10^{12} mol yr^{-1} or 219 μmol L^{-1}), does not enable to sustain [O_2] to the level of saturation (~246 μmol L^{-1} at $T = 28$°C) because of the intense rate of mineralization. The balance between inputs and outputs relative to O_2 and CO_2 seems to be likely achieved before the junction of the major tributaries so that [O_2] and [CO_2] remain relatively stable along their course in the floodplains. The rate of CO_2 outgassing ΦR is controlled by the surface of submerged land (FA) and the exchange coefficient K at the interface river–atmosphere, according to Fick's law. The main factor driving the magnitude of chemical and isotopic shifts between incoming and outgoing signals is the ratio submerged area/river discharge (FA/Qt). The submerged area determines the magnitude of CO_2 release in river water, whereas the discharge determines the river dilution. The shift mainly depends on the extension of flooded area. Considering the mean coverage of flooded areas equals 34 000 km^2 for the overall studied reach (from Richey et al. 2002), the flux of mineralization seems to be sustained by the net primary production of river corridors, estimated to be $2.987 \times 10^{12}/(3.4 \times 10^{10}) = 87.9$ mol C m^{-2} yr^{-1} = 1054 g C m^{-2} yr^{-1}. This value is of the same order of magnitude as net primary production values for tropical wetlands and várzea forests (e.g., Piedade et al. 2001).

The striking fact is the huge magnitude of the rates of reactions of the 14 considered processes compared to the rates of exportation of the studied chemical species. This can be interpreted as the result of a very fast turnover, especially for

DIN, DON, POCC, and PONC and to a lesser extent for POCF, PONF, and DIC. According to Mayorga et al. (Mayorga et al. 2005), the flux of mineralization involves contemporary organic carbon (whose $\Delta^{14}C$ is high). The rapid cycling of autochthonous carbon, mainly composed of aquatic várzeas grasses incorporated to floodplain sediments, fuels respiration and sustains CO_2 supersaturation. Actually, the dating of organic matter using ^{14}C signatures (Hedges et al. 1986b; Mayorga et al. 2005) suggests that DOC and overall POCF are actually much more stable than Figure 10 might indicate. This apparent discrepancy between model outcomes and isotopic dating simply indicates that POCF and DOC do not display uniform reactivity. Within each size fraction, at least two compartments must be distinguished: 1) a labile autochthonous compartment mainly fuelled by local sources by means of aquatic and aerial photosynthesis (in the floodplains) and 2) a refractory allochthonous soil-derived compartment subtracted to biological transformations by means of sorption onto fine suspended sediments.

5. Conclusions

The magnitude and direction of the water exchanges between the Amazon River and its floodplains strongly influences the sedimentary and chemical signals measured over the studied reach. The floodplains constitute widespread sites where major biotic and abiotic processes affecting the dynamics of transiting materials occur: sedimentation, remobilization of sediments, organic matter decay, CO_2 outgassing, etc.

The methodology applied here allowed us 1) to reconstitute the logic of acquisition of river water composition by revisiting the interpretation given to the seasonal (potentially compensated) and annual (net removal or net gain) defaults of mass balance closure; 2) to identify major factors driving fundamental biogeochemical cycles and chemical baseline of large river basins; 3) to reevaluate the carbon budget of large river basins; and 4) to measure the importance of biotic processes (organic matter decay, aquatic photosynthesis, etc) and abiotic processes (e.g., DOM sorption, CO_2 outgassing, methane emission) operating in flooded plains, on the chemistry of river water.

The climatic fluctuations modify the contribution of flow components to the total river discharge without changing their individual composition, unless long-term variations arise. For this reason, the specific impact of humans (disregarding human-induced climate changes) can be separated from the action of climate provided that the characteristics of hydrological and biogeochemical end members are well captured and that the magnitude of biogeochemical transformations is accurately established (by modeling) for two distinct periods with contrasted human pressure. Thus, with a sound sampling strategy like CAMREX, one may eventually estimate retrospectively, provided that sampling strategy is adapted, the impacts of anthropogenic activities (land-use changes, management of river corridors, etc), which are susceptible to modify the chemical features of flow components. Despite the unavoidable confusions (i) due to the inaccuracies of the chemical dataset, (ii) due to the lack of samples for each station, and (iii) despite the numerous simplifications and hypotheses required to implement the process-based model, the strategic approach developed here provides a fair picture of the biogeochemistry of the Amazonian floodplains.

Acknowledgments. This work was funded by the Brazilian FAPESP agency by way of a postdoctoral fellowship (2005/58884-5) associated to the project entitled "A large-scale synthetic model applied to the hydroclimatology and eco-geodynamics of the Amazon River basin." This study benefited from insightful comments and suggestions provided by two anonymous referees whose very careful review contributed indeed to improve substantially the quality of the language and the clarity of the thinking. Many thanks are addressed to Prof. Yves Tardy, retired in Toulouseshire (France), and to Roger Brouet, former director of the experimental farm of Le Pradel (Aubenas, France), for their unconditional support during the Ph.D. thesis of VB.

References

Ahad, J. M. E., J. A. C. Barth, R. S. Ganeshram, R. G. M. Spencer, and G. Uher, 2008: Controls on carbon cycling in two contrasting temperate zone estuaries: The Tyne and Tweed, UK. *Estuarine Coastal Shelf Sci.,* **78,** 685–693.

Amon, R. M. W., and R. Benner, 1996: Photochemical and microbial consumption of dissolved organic carbon and dissolved oxygen in the Amazon River system. *Geochim. Cosmochim. Acta,* **60,** 1783–1792.

Aucour, A. M., S. M. F. Sheppard, O. Guyomar, and J. Wattelet, 1999: Use of ^{13}C to trace origin and cycling of inorganic carbon in the Rhône river system. *Chem. Geol.,* **159,** 87–105.

Aufdenkampe, A. K., 2002: The role of sorptive processes in the organic carbon and nitrogen cycles of the Amazon River basin. Ph.D thesis, University of Washington, 164 pp.

——, J. I. Hedges, A. V. Krusche, C. Llerena, and J. E. Richey, 2001: Sorptive fractionation of dissolved organic nitrogen and amino acids onto sediments within the Amazon basin. *Limnol. Oceanogr.,* **46,** 1921–1935.

Barth, J. A. C., and J. Veizer, 1999: Carbon cycle in the St. Lawrence aquatic ecosystems at Cornwall (Ontario), Canada: Seasonal and spatial variations. *Chem. Geol.,* **159,** 107–128.

——, A. A. Cronin, J. Dunlop, and R. M. Kalin, 2003: Influence of carbonates on the riverine carbon cycle in an anthropogenically dominated catchment basin: Evidence from major elements and stable carbon in the Lagan River (N. Ireland). *Chem. Geol.,* **200,** 203–216.

Benner, R., S. Opsahl, G. Chin-Leo, J. E. Richey, and B. R. Forsberg, 1995: Bacterial carbon metabolism in the Amazon River system. *Limnol. Oceanogr.,* **40,** 1262–1270.

Bernoux, M., M. D. S. Carvalho, B. Volkoff, and C. C. Cerri, 2002: Brazil's soil carbon stocks. *Soil Sci. Soc. Amer. J.,* **66,** 888–896.

Brown, S., and A. Lugo, 1992: Above ground biomass estimates for tropical moist forest of the Brazilian Amazon. *Interciencia,* **17,** 8–18.

Brunet, F., D. Gaiero, J. L. Probst, P. J. Depetris, F. Gauthier Lafaye, and P. Stille, 2005: $\delta^{13}C$ tracing of dissolved inorganic carbon sources in Patagonian rivers (Argentina). *Hydrol. Proc.,* **19,** 3321–3345.

Bushaw, K. L., and Coauthors, 1996: Photochemical release of biologically available nitrogen from aquatic dissolved organic matter. *Nature,* **381,** 404–407.

Bustillo, V., 2007: A large-scale synthetic model applied to the hydroclimatology and eco-geodynamics of the Amazonian basin. FAPESP Rep. 2005-58884-5, 93 pp.

——, R. L. Victoria, J. M. S. Moura, D. Victoria, A. M. A. Toledo, and E. Collicchio, 2010: Biogeochemistry of the Amazonian floodplains. Insights from six end-member mixing models. *Earth Interactions,* **14.** [Available online at http://EarthInteractions.org.]

Cameron, E. M., G. E. M. Hall, J. Veizer, and H. R. Krouse, 1995: Isotopic and elemental hydrogeochemistry of a major river system: Fraser River, British Columbia, Canada. *Chem. Geol.,* **122,** 149–169.

Cole, J. J., N. F. Caraco, G. W. Kling, and T. K. Kratz, 1994: Carbon dioxide super saturation in the surface waters of lakes. *Science,* **256,** 1568–1570.

Craig, H., 1954: Geochemical implications of the isotopic composition of carbon in ancient rocks. *Geochim. Cosmochim. Acta,* **6,** 186–196.

Devol, A. H., P. D. Quay, J. E. Richey, and L. A. Martinelli, 1987: The role of gas exchange in the inorganic carbon, oxygen, and ^{222}Rn budgets of the Amazon River. *Limnol. Oceanogr.,* **32,** 235–248.

——, J. E. Richey, W. A. Clark, S. L. King, and L. A. Martinelli, 1988: Methane emissions to the troposphere from the Amazon floodplain. *J. Geophys. Res.,* **93,** 1583–1592.

——, B. R. Forsberg, J. E. Richey, and T. P. Pimentel, 1995: Seasonal variation in chemical distributions in the Amazon (Solimões) River: A multiyear time series. *Global Biogeochem. Cycles,* **9,** 307–328.

Doctor, D. H., C. Kendall, S. D. Sebestyen, J. B. Shanley, N. Ohte, and E. W. Boyer, 2008: Carbon isotope fractionation of dissolved inorganic carbon (DIC) due to outgassing of carbon dioxide from a headwater stream. *Hydrol. Processes,* **22,** 2410–2423.

Ertel, J. R., J. I. Hedges, A. H. Devol, and J. E. Richey, 1986: Dissolved humic substances of the Amazon River system. *Limnol. Oceanogr.,* **31,** 739–754.

Faure, G., 1977: *Isotope Geology.* John Wiley and Sons, 464 pp.

Fisher, T. R., 1979: Plankton and primary production in aquatic systems of the central Amazon basin. *Comp. Biochem. Physiol.,* **62,** 31–38.

Hedges, J. I., W. A. Clark, P. D. Quay, J. E. Richey, A. H. Devol, and U. M. Santos, 1986a: Compositions and fluxes for particulate organic material in the Amazon River. *Limnol. Oceanogr.,* **31,** 717–738.

——, and Coauthors, 1986b: Organic carbon-14 in the Amazon River system. *Science,* **231,** 1129–1131.

——, G. L. Cowie, J. E. Richey, P. D. Quay, R. Benner, and M. Strom, 1994: Origins and processing of organic matter in the Amazon River as indicated by carbohydrates and amino acids. *Limnol. Oceanogr.,* **39,** 743–761.

Leenheer, J. A., 1980: Origin and nature of humic substances in the waters of the Amazon River basin. *Acta Amazonica,* **10,** 513–526.

Martinelli, L. A., R. L. Victoria, P. B. Camargo, M. Piccolo, L. Mertes, J. E. Richey, A. H. Devol, and B. R. Forsberg, 2003: Inland variability of carbon-nitrogen concentrations and δ^{13}C in Amazon floodplain (várzea) vegetation and sediment. *Hydrol. Processes,* **17,** 1419–1430.

Mayorga, E., and A. K. Aufdenkampe, 2002: The processing of bioactive elements by the Amazon River system. *The Ecohydrology of South American Rivers and Wetlands,* M. E. McClain, Ed., IAHS Press, 1–24.

——, ——, C. A. Masiello, A. V. Krusche, J. I. Hedges, P. D. Quay, and J. E. Richey, 2005: Young organic matter as a source of CO_2 outgassing from Amazonian Rivers. *Nature,* **436,** 538–541.

Moreira-Turcq, P., P. Seyler, J. L. Guyot, and H. Etcheber, 2003a: Exportation of organic carbon from the Amazon River and its main tributaries. *Hydrol. Processes,* **17,** 1329–1344.

——, ——, ——, and ——, 2003b: Characteristics of organic matter in the mixing zone of the Rio Negro and Rio Solimões of the Amazon River. *Hydrol. Processes,* **17,** 1393–1404.

Moura, J. M., C. S. Martens, M. Z. Moreira, R. L. Lima, I. C. G. Sampaio, H. P. Mendlovitz, and M. C. Menton, 2008: Spatial and seasonal variations in the stable carbon isotopic composition of methane in stream sediments of eastern Amazonia. *Tellus,* **60B,** 21–31.

Piedade, M. T. F., W. J. Junk, and S. P. Long, 1991: The productivity of the C_4 grass *Echinochloa polystachya* in the Amazon floodplain. *Ecology,* **72,** 1456–1463.

——, M. Worbes, and W. J. Junk, 2001: Geoecological controls on elemental fluxes in communities of higher plants in Amazonian floodplains. *The Biogeochemistry of the Amazon Basin,* M. E. McClain, R. L. Victoria, and J. Richey, Eds., Oxford University Press, 209–234.

Quay, P. D., D. O. Wilbur, J. E. Richey, J. I. Hedges, A. H. Devol, and R. L. Victoria, 1992: Carbon cycling in the Amazon River: Implications from the ^{13}C compositions of particles and solutes. *Limnol. Oceanogr.,* **37,** 857–871.

——, ——, ——, A. H. Devol, R. Benner, and B. R. Forsberg, 1995: The $^{18}O/^{16}O$ of dissolved oxygen in rivers and lakes in the Amazon basin: A tracer of respiration and photosynthesis. *Limnol. Oceanogr.,* **40,** 718–729.

Richey, J. E., R. H. Meade, E. Salati, A. H. Devol, C. F. Nordin, and U. M. Santos, 1986: Water discharge and suspended sediment concentrations in the Amazon River: 1982–1984. *Water Resour. Res.,* **22,** 756–764.

——, A. H. Devol, S. C. Wofsy, R. L. Victoria, and M. N. G. Ribeiro, 1988: Biogenic gases and the oxidation and reduction of carbon in Amazon River and floodplain waters. *Limnol. Oceanogr.,* **33,** 551–561.

——, L. A. K. Mertes, T. Dunne, R. L. Victoria, B. R. Forsberg, A. C. N. S. Tancredi, and E. Oliveira, 1989: Sources and routing of the Amazon River flood wave. *Global Biogeochem. Cycles,* **3,** 191–204.

——, J. M. Melack, A. K. Aufdenkampe, M. V. Ballester, and L. L. Hess, 2002: Outgassing from Amazonian rivers and wetlands as a large tropical source of atmospheric CO_2. *Nature,* **416,** 617–620.

——, A. K. Aufdenkampe, S. Remington, A. V. Krusche, and E. Mayorga, 2004: ROMBUS: A model of DOM mobilization and reaction. *Ocean Research Conf.,* Honolulu, Hawaii, American Society of Limnology and Oceanography, 1037.

——, R. L. Victoria, J. I. Hedges, T. Dunne, L. A. Martinelli, L. Mertes, and J. Adams, 2008: Pre-LBA Carbon in the Amazon River Experiment (CAMREX) data. Oak Ridge National Laboratory Distributed Active Archive Center. [Available online at http://daac.ornl.gov/cgi-bin/dsviewer.pl?ds_id=904.]

Salati, E., R. Sylvester-Bradley, and R. L. Victoria, 1982: Regional gains and losses of nitrogen in the Amazon basin. *Plant Soil,* **67,** 367–376.

Stevenson, F. J., 1994: *Humus Chemistry: Genesis, Composition, Reactions*. 2nd ed. John Wiley and Sons, 512 pp.

Tan, F. C., and J. M. Edmond, 1993: Carbon isotope geochemistry of the Orinoco basin. *Estuarine Coastal Shelf Sci.,* **36,** 541–547.

Tardy, Y., V. Bustillo, C. Roquin, J. Mortatti, and R. L. Victoria, 2005: The Amazon. Biogeochemistry applied to the river basins management: Part I. Hydroclimatology, hydrograph separation, mass transfer balance, stable isotopes and modelling. *Appl. Geochem.,* **20,** 1746–1829.

——, C. Roquin, V. Bustillo, M. Moreira, L. A. Martinelli, and R. L. Victoria, 2009: *Carbon and Water Cycles: Amazon River Basin: Applied Biogeochemistry.* Atlantica, 479 pp.

Victoria, R. L., L. A. Martinelli, P. C. O. Trivelin, E. Matsui, B. R. Forsberg, J. E. Richey, and A. H. Devol, 1992: The use of stable isotopes in studies of nutrient cycling: Carbon isotope composition of Amazon varzea sediments. *Biotropica,* **24,** 240–249.

Wissmar, R. C., J. E. Richey, R. F. Stallard, and J. M. Edmond, 1981: Plankton metabolism and carbon processes in the Amazon River, its tributaries, and floodplain waters, Peru–Brazil, May–June 1977. *Ecology,* **62,** 1622–1633.